CRYSTAL GROWTH & DESIGN

Article

pubs.acs.org/crystal

Nanographite Synthesized from Acidified Sucrose Microemulsions under Ambient Conditions

Natasha J. Hargreaves and Sharon J. Cooper*

Durham University, Department of Chemistry, South Road, Durham, DH1 3LE, United Kingdom

Supporting Information

ABSTRACT: We show here that nanographite can be synthesized at room temperature and pressure through a simple process of acidifying sucrose microemulsions. This is in contrast to conventional wisdom, which stipulates that graphite can only be produced using high temperatures. Natural graphite arises via progressive metamorphisms of carbonaceous material subjected to temperatures above ∼600 K and pressures >2 kbar. Synthetic pyrolytic graphite requires temperatures >2500 K, and even nanographite formation from amorphous carbons requires temperatures >850 K. Our synthesis route utilizes the dehydration of sucrose by concentrated sulfuric acid, a variant of the well-known carbon black snake experiment, which produces an amorphous carbonaceous product. Crucially, though, we conduct the reaction in nanometer-sized microemulsion droplets to exert control over the reaction and sheet stacking process. This ensures that only sufficiently pristine graphene nanosheets can stack, thereby producing nanographite in a simple one-step synthesis under ambient conditions. The primary nanographitic particles of size ∼3−30 nm stack in crystallographic registry to form larger 250 nm- to μm-sized nanographitic aggregates. The amount of nanographite produced from the microemulsions is limited, however, because the sucrose concentration must be kept very low to slow the reaction kinetics. Hence, this is not a viable method for commercially producing nanographite.

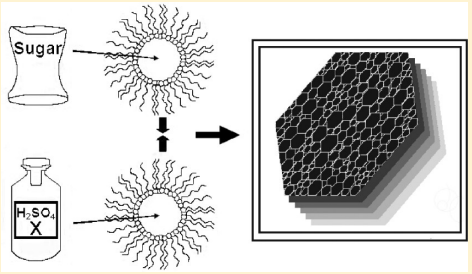

INTRODUCTION

Graphite is a crystalline allotrope of carbon that is thermodynamically stable under ambient conditions and consists of stacked graphene layers. Graphene is a zero band gap semiconductor material with intrinsic properties of remarkable charge mobility, high mechanical strength, and excellent thermal conductivity. These attributes may ultimately deliver significant benefits in areas such as optoelectronics, energy storage, and molecular sensing either intrinsically or through doping.[1−4] It is widely accepted that graphite synthesis requires ultrahigh temperatures or a combination of high temperature and pressure. Natural graphite arises via progressive metamorphisms of carbonaceous material subjected to temperatures above ∼600 K and pressures >2 kbar with the degree of crystallinity correlated with increasing metamorphic grade.[5] Synthetic pyrolytic graphite and highly oriented pyrolytic graphite (HOPG) require temperatures >2500 K and ∼3300 K, respectively.[6] Nanographite can be formed by heating amorphous carbons but even here temperatures >850 K are required.[7]

In contrast, humins, an amorphous carbonaceous material containing residual oxygens and hydrogens, are of little value but can be readily produced under ambient conditions. The familiar carbon black snake school experiment provides one such synthesis route to humins. This uses concentrated sulfuric acid to dehydrate sucrose, a highly exothermic reaction that vaporizes the water causing the carbonaceous product, the black snake, to be pushed out of the reaction vessel. However, the overall reaction suggested to children, namely, $C_{12}H_{22}O_{11} \rightarrow 12C + 11H_2O$ does not go to completion. Instead, the carbonaceous product rapidly becomes insoluble, precipitating as amorphous humins. The elemental composition of the humins is typically ∼55−65% carbon, 4−5% hydrogen, and 30−40% oxygen[8] with a significant proportion of sp^2 carbons. The humin structure mainly consists of furanic segments with aliphatic linkages decorated with carboxylic and ketone groups.[9] The reaction is thought to arise via a 5-hydroxymethylfurfural (5-HMF) intermediate,[8,10,11] which can polymerize to form humins and hydrolyze in a side reaction to give levulinic and formic acids. Our aim was to determine whether the carbon black snake experiment could be forced to go to completion in a simple one-step synthesis under ambient temperature conditions, thereby producing a graphitic rather than humin product. We have achieved this by using the 3D nanoconfinement of microemulsions to exert control over both the chemical reaction and stacking processes.

The difficulty in converting carbohydrates into graphite is well-known. Indeed, in 1951, Rosalind Franklin designated sucrose as a nongraphitizable carbon because, upon pyrolysis, less than 5% of graphitic carbons were evident in the product, even at temperatures of 3273 K.[12] More recently, monolayer pristine graphene has been grown from solid carbon sources such as sucrose and PMMA at elevated temperatures of 1073 K on top of a copper foil.[13] Glucose has been calcined at 873 K in the presence of dicyandiamide to produce graphene via growth

Received: December 11, 2015
Revised: April 29, 2016
Published: May 9, 2016

DOI: 10.1021/acs.cgd.5b01753
Cryst. Growth Des. 2016, 16, 3133−3142

on a sacrificial carbon nitride template, which was subsequently removed by heating to 1273 K.[14] In addition, graphitic nanocoils have been synthesized from sucrose and glucose hydrochar in the presence of nickel nanoparticle catalysts, but again high temperatures were required with the graphitization process only commencing above 973 K.[15] Obtaining graphitic carbons from the humins produced after the reaction of sucrose with sulfuric acid is also problematic; the extensive furanic network in the humins needs to be converted into a graphitic structure composed of fused benzene rings. Advanced solid state NMR analysis on glucose treated with sulfuric acid shows that large polycondensed aromatic units containing more than 5 rings only occur after thermal annealing at temperatures significantly above 623 K.[16] The development of graphitic crystallinity requires even higher temperature; amorphous carbons, such as humins, need temperatures of 873 K or more, even in the presence of transition metal catalysts.[17] In our microemulsion methodology, the development of an extensive furanic network is hindered by the limited rate at which the carbonaceous sheets can grow. We suspect it is this that substantially aids the room temperature formation of nanographite, though the actual reaction mechanism is yet to be elucidated.

The use of carbohydrates to produce luminescent carbon dots has been reported recently using elevated temperatures.[18] The carbon dots were produced using ambient temperature dehydration of sucrose with sulfuric acid, followed by refluxing of the deposited particles with nitric acid; passivation of the nanoparticles was achieved by adding 4,7,10-trioxa-1,13-tridecanediamine and heating to 393 K under a N_2 atmosphere for 72 h.[18] The ∼5 nm particles had a mean interlayer spacing of ∼3.4 Å, which is similar to that of graphite, but lacked 3D crystalline order. The room temperature reduction of graphene oxide to graphene has been reported recently using lithium aluminum tetrahydride with phosphorus tribromide[19] and zinc with mineral acid.[20] However, this is the first report demonstrating how nanographitic particles can be produced at room temperature by a bottom-up synthesis route using microemulsions.

Our nanographitic product consists of smaller ∼3−30 nm few-layer graphene building blocks, denoted primary particles, which stack in a crystallographic registry to give a mesocrystal-type structure. A mesocrystal is a three-dimensional array of iso-oriented single crystal particles of size 1−1000 nm. The labeling of crystals as "mesocrystals" can be erroneous.[21] To be categorized as a mesocrystal, there must be unambiguous evidence of crystalline subunits within the crystal that pack in the crystallographic registry so that their diffraction patterns resemble those of single crystals. We consider our nanographitic aggregates as mesocrystal-like in recognition that our primary particles vary in size and may not be entirely crystalline; rather, the edges of our graphene sheets will often be decorated with oxygenated groups, and some of the primary particle interior may contain furan rings as well as fused benzene rings. Nevertheless, our primary particles have sufficient crystalline character to stack in a crystallographic registry and produce a single crystal-type electron diffraction pattern. Microemulsions have recently been used to grow mesocrystals of dipicolinic acid.[22] The subunit nanocrystals had a size commensurate with those of the droplets, illustrating that microemulsions can help promote the formation of mesocrystals.

EXPERIMENTAL SECTION

Materials. Chemicals were used as supplied and were as follows: cetyltrimethylammonium chloride (CTAC) (99%, Acros Organics), sulfuric acid (>95%, Fisher Scientific), Silver Spoon granulated sugar (Tate & Lyle), cyclohexane (99% GLC Specified, Fisher Scientific), and pentan-1-ol (ACS reagent ≥99%, Aldrich). Ultra high purity (UHP) water with a resistivity of 18.2 MΩ cm was obtained from a Sartorius arium comfort water purifier system.

Nanographite Synthesis. The nanographitic particles were synthesized via two different microemulsion methodologies: the mixed microemulsion method and the sucrose crystal method.

Nanographite Synthesis by the Mixed Microemulsion Method. In the first method, denoted the mixed microemulsion method, two separate microemulsions containing sulfuric acid and sucrose solution were mixed. The sulfuric acid microemulsion comprised 20 μL of a 75 or 95 wt % sulfuric acid in a 1 g aliquot of surfactant solution. The surfactant solution contained cetyltrimethylammonium chloride (CTAC) in cyclohexane and pentan-1-ol in a mass ratio of 1:7.8:2. The sucrose microemulsion comprised 20 μL of aqueous sucrose (0.1−30 wt %) in a 1 g aliquot of the same surfactant solution. Equal volumes of the aqueous sucrose microemulsion and the sulfuric acid microemulsion were mixed by being shaken by hand or vortexed. This produced a clear isotropic phase, which was then left under ambient conditions to synthesize the nanographite.

Nanographite Synthesis by the Sulfuric Acid Microemulsion and Sucrose Crystal Method. A second synthesis method was adopted to provide more product. In this method, sucrose crystals were added to a sulfuric acid microemulsion. The vials were left for a month, during which time black material deposited on the bottom of the vials.

Characterization of Nanographite from the Mixed Microemulsion Method. After 24 h, drops of the microemulsions were typically deposited onto holey carbon TEM copper grids (Agar Scientific), left to dry, washed with cyclohexane and then an acetone and water solution containing 75 wt % acetone, and left to dry before examination using TEM. For the Raman microscopy, AFM, and ESEM studies, drops of the microemulsions were deposited onto silicon SiO_2 300 nm pink wafers and left to dry. Residual surfactant and sulfuric acid were removed by repeatedly washing under water and ethanol sonication.

Characterization of Nanographite from the Sulfuric Acid Microemulsion and Sucrose Crystal Method. The black deposit was collected, washed with the acetone and water solution, and air dried. For Raman microscopy and X-ray diffraction (XRD) studies, the washed deposit was placed on a (111) silicon wafer. For TEM studies, a small portion of the washed deposit was redispersed in acetone and water through vortexing or sonication. A few drops of the dispersion were placed onto holey carbon TEM grids and left to dry.

Characterization Techniques. TEM studies used a JEOL 2100F FEG-200 kV TEM operating at 80 kV. The Raman microscopy was conducted on a Jobin Yvon Horiba LabRAM spectrometer in a back scattered confocal configuration using He Ne (633 nm, 1.96 eV) laser excitation. AFM studies employed a Veeco Multimode AFM with a Nanoscope IV controller in tapping mode. For the ESEM studies, the samples were gold spin-coated on the wafers and placed in a Hitachi SU70 FEG-SEM operated at 10 kV using secondary electron detection. XRD studies were conducted on a D8 Bruker diffractometer with cross-coupled Göbel mirrors and pinhole collimation for point focus geometry using a sealed tube X-ray source operated at 30 kV and 10 mA to produce Cu Kα radiation of wavelength 1.54 Å. The X-ray incidence angle was fixed at 10°. X-rays scattered from the sample were detected with a Hi-Star 2D multiwire detector (effective pixel size of 100 μm).

Microemulsion Droplet Size Analysis. Small angle X-ray scattering (SAXS) measurements were performed on our in-house Bruker Nanostar, with cross-coupled Göbel mirrors and pinhole collimation, using a sealed tube X-ray source operated at 40 kV and 35 mA to produce the Cu Kα radiation. The SAXS camera was fitted with a Hi-star 2D multiwire detector. Samples were contained in 2 mm glass capillaries. The optics and sample chamber were under vacuum to minimize air scatter. Scattering files were background subtracted using the solvent-filled capillary and then integrated to give the one-dimensional scattering intensity function $I(q)$, where q is the length of

DOI: 10.1021/acs.cgd.5b01753
Cryst. Growth Des. 2016, 16, 3133−3142

the scattering vector defined by $q = (4\pi/\lambda)\sin\theta$ with λ the wavelength and 2θ the scattering angle. The sample-to-detector distance was 650 mm, which provided a q range of 0.2−3.2 nm^{-1}. GIFT analysis[23] of the scattering function was used to determine a mean size for the microemulsion droplets (Supporting Information).

RESULTS AND DISCUSSION

Mixed Microemulsion Synthesis Methodology. Figure 1 displays a schematic of our nanographite synthesis route produced by mixing two microemulsions, one containing sulfuric acid and the other containing a solution of sucrose. Droplet microemulsions comprise thermodynamically stable, nm-sized droplets of a liquid, or solution, dispersed in an immiscible liquid or solution. The droplets undergo collisions, the most energetic of which allow transient droplet dimer formation with concomitant exchange of droplet interior content so that the sucrose and sulfuric acid mix and react to produce carbonaceous particles contained within the droplets. Growth of the carbonaceous primary particles will continue (albeit hindered by the physical constraint of the microemulsion droplet interface) until the reactants are depleted. Importantly, this particle growth rate is significantly reduced compared to that of bulk solution where the reactants are spatially unrestricted, and it is this that enables the formation of nanographitic aggregates rather than humins. The formation of nanographite via this novel microemulsion route is similar to a thermodynamic control of crystallization methodology.[24,25]

A reversible reaction pathway is a prerequisite for thermodynamic control. This reversibility ensures that less stable but quicker growing nuclei readily dissolve, thus enabling an equilibrium population of nuclei dominated by the most stable form to be achieved. The dehydration of sucrose by the sulfuric acid is essentially irreversible however. Instead, it is the reversibility of the stacking process for these small nm-sized carbonaceous particles that helps to achieve the more stable nanographitic, rather than humin, product.

The tendency of graphene and carbonaceous particles to stack/aggregate irreversibly will be a function of their size, shape, chemical and structural purity, and strength of the surrounding acid; pristine graphene sheets will stack irreversibly at a smaller size in the concentrated sulfuric acid than highly defective sheets or carbonaceous spherical particles containing residual oxygen and hydrogen. This is, for example, exemplified by graphite oxide dispersing rapidly in water via sonication,[26] whereas graphite requires 2 days of stirring in chlorosulfonic acid to produce graphene.[27]

The dehydration of sucrose by concentrated sulfuric acid in bulk solution produces a rapid polymerization such that the carbonaceous products (which can be viewed as highly defective and doped graphene cross-linked sheets incorporating oxygen and hydrogen) rapidly attain sizes at which they can stack irreversibly with these defects and dopants incorporated. Hence, insoluble humins are precipitated. In contrast, the growth rate of a carbonaceous sheet in a microemulsion droplet is significantly reduced, limited by the scarce amount of reactants within the droplet and by restricted access to further reactant via transient dimer formation. Consequently, the nm-sized defective sheets in the droplets cannot acquire further reactant and grow at the rapid rate under which irreversible stacking arises. Crucially, they remain dispersed in the nanosolution, continually subjected to an excess of sulfuric acid so that further dehydration occurs until stackable, essentially pristine graphene sheets are formed (Figure 1). Accordingly, the population of stacked sheets will reach a (near) equilibrium dominated by nanoparticles containing a few layers of essentially pristine graphene.

The graphitic nanoparticles will continue to acquire additional reactant and, subsequently, additional graphene sheets via droplet collisions to form larger graphitic nanoparticles of size ∼3−30 nm; these are denoted as primary nanographitic particles (Figure 1). Importantly, these primary particles remain

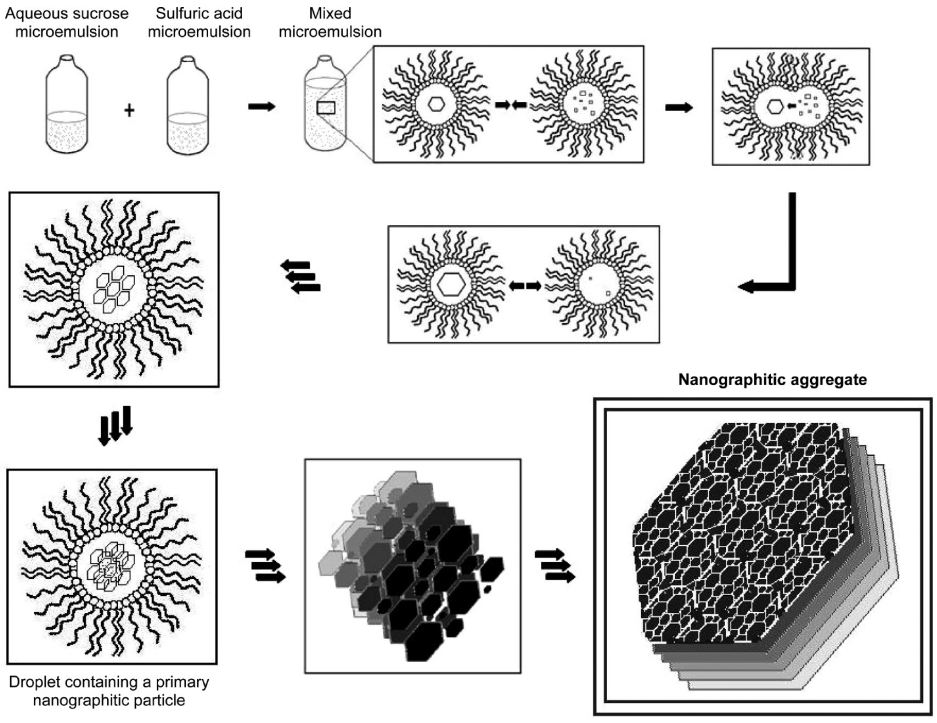

Figure 1. Schematic diagram depicting the nanographite synthesis mechanism.

DOI: 10.1021/acs.cgd.5b01753
Cryst. Growth Des. 2016, 16, 3133−3142

bathed in sulfuric acid (with a stabilizing surfactant layer). The close approach of these nanographitic particles will lead to further ordered stacking until ultimately μm-sized particles are produced; these are denoted nanographitic aggregates (Figure 1).

Thermodynamic control is achieved by sufficiently restricting the graphene sheet growth rate using aqueous sucrose concentrations of 0.25−1 wt % within the microemulsions held at room temperature. The microemulsions remain colorless at these low sucrose concentrations but show increased darkening as the dehydration reaction proceeds in sucrose concentrations of >5 wt % (Figure 2). The composition of all the microemulsions studied in terms of the molarity, mass fractions, and volume fractions of their constituent chemicals is shown in the Supporting Information Tables 1−3.

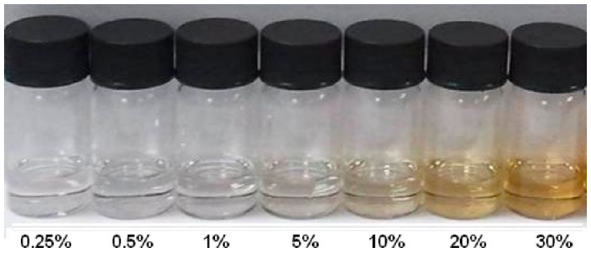

Figure 2. Photograph of mixed microemulsions after 7 days at room temperature showing increased darkening due to the sucrose dehydration and polymerization reaction for the >5 wt % aqueous sucrose concentrations. The sucrose wt % is labeled below the vials.

Primary Nanographitic Particles. SAXS analysis (Supporting Information SAXS results and Figure S1) shows that the mixed microemulsions contained approximately spherical droplets with a mean hydrophilic core radius of ∼1.9 nm. TEM analysis on drops of the microemulsions placed on holey carbon grids established that a nanographitic product can be obtained provided the sucrose content is kept at or below 1 wt % of the aqueous phase. Representative TEM data obtained from eight different mixed microemulsion samples containing 0.25−1% sucrose in the aqueous phase are shown in Figures 3 and 4 and Figures S2−S4. In the absence of sucrose, no nanographitic particles were found during TEM analysis on drops from microemulsions left for 1 month, establishing that the sucrose is the source of the nanographitic particles and not the much larger quantities of CTAC surfactant and pentanol cosurfactant. Furthermore, the bulk sulfuric acid and sucrose reaction only produces the expected amorphous humins with no evidence of any crystalline material being found by TEM. Indeed, although it is well-known that largely amorphous carbons can contain graphitic material because the reaction conditions have involved high temperatures and/or pressures, i.e., a graphitization trajectory has been followed, the occurrence of graphitic material from the room temperature reaction between sucrose and sulfuric acid has never been reported previously. Consequently, the occurrence of the nanographitic particles from the room temperature microemulsion synthesis route demonstrates a fundamental ordering effect on the synthesis that is absent in the bulk route.

Figure 3 shows representative TEM images of the primary nanographitic particles of size ∼3−30 nm. Fast Fourier transforms (FFTs) of the high resolution images of the primary particles show the hexagonal pattern expected for graphite (Figure 3b) with only trace oxygen in the accompanying

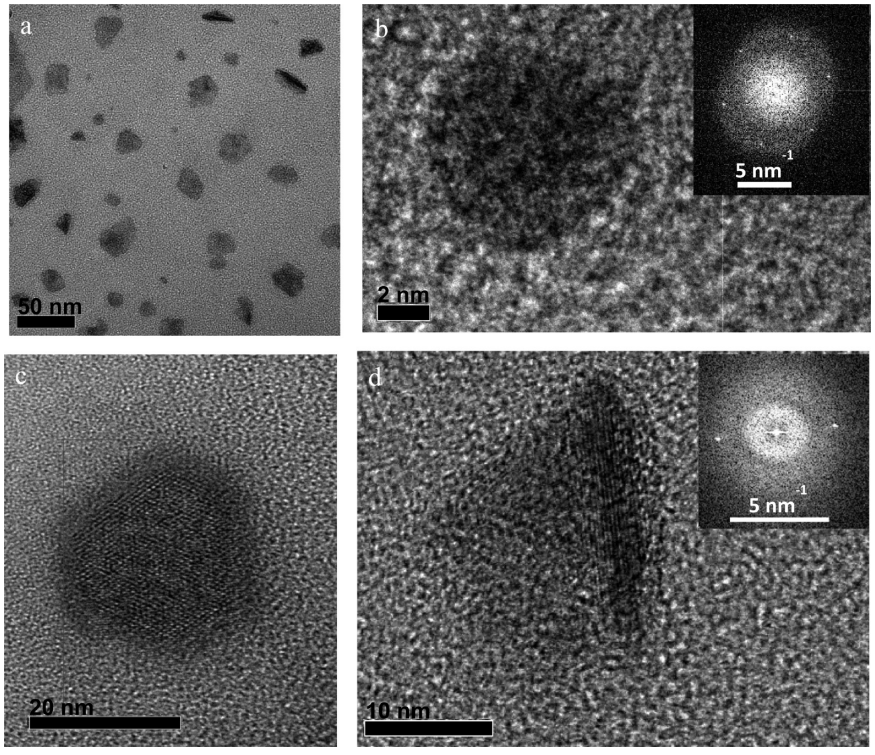

Figure 3. TEM of the primary nanographitic particles synthesized from 0.25 to 1 wt % of aqueous sucrose and sulfuric acid-mixed microemulsions. (a) Bright field image of a group of ∼3−30 nm particles. (b) High resolution image (HREM) of an 8 nm particle. The FFT (inset) shows the expected graphitic 0.213 nm hexagonal pattern. (c) HREM of a hexagonal ∼25 nm particle. (d) An ∼15 nm particle folded on the right-hand side, showing 15 layers. The FFT (inset) gives the expected 0.34 nm interlayer graphite spacing.

DOI: 10.1021/acs.cgd.5b01753
Cryst. Growth Des. 2016, 16, 3133−3142

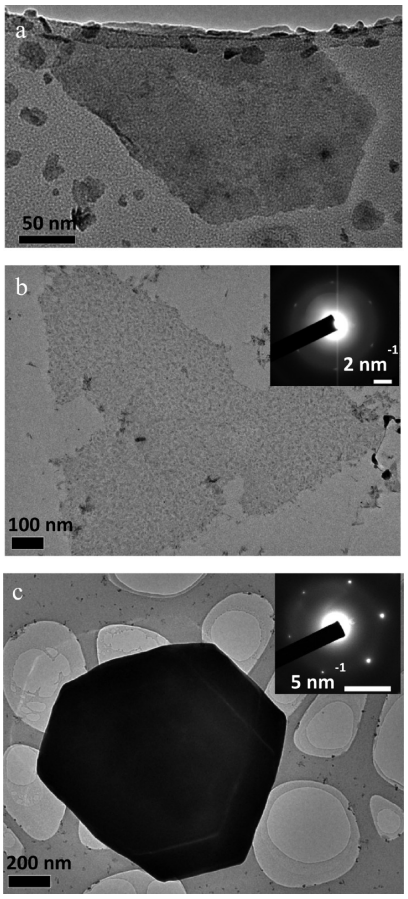

Figure 4. TEM of the nanographitic aggregates synthesized from 0.25 to 1 wt % aqueous sucrose and sulfuric acid-mixed microemulsions. (a) Bright field image of an ~250 nm particle surrounded by smaller primary particles. (b) Bright field image of a thin and patchy μm-sized particle. Its weak electron diffraction pattern (inset) shows the expected 0.213 nm hexagon. (c) A μm-sized particle; its electron diffraction pattern (inset) shows the expected 0.213 nm hexagon.

energy-dispersive X-ray (EDX) spectra (Figure S2b). The trace oxygen quantities shown in the EDX spectra are similar to those found in a commercial multilayer graphene sample with an elemental composition of 86.7% carbon, 0.6% hydrogen, and 12.7% oxygen (Figure S5e) and considerably less than the amount found in the EDX of the amorphous product from the bulk sulfuric acid and sucrose reaction for which the elemental composition was 54.5% carbon, 1.8% hydrogen, and 43.7% oxygen (Figure S6c). Many FFTs of our 3−30 nm primary particles also reveal a $\sqrt{3}$ R30° supercell,[28] which we attribute to surface-adsorbed sulfuric acid given that trace sulfur and oxygen are present in the accompanying EDX spectra (Figures S2e,f).

In folded regions of the nanoparticles (Figure 3d), the FFTs consistently show the 0.34 nm graphite interlayer spacing. This further demonstrates that the dehydration of sucrose is virtually complete; the residual oxygen is confined to the sheet edges, where it will not hinder the stacking of the essentially pristine graphene sheets. Significant levels of residual oxygen and hydrogen within the graphene sheets would have given a product akin to graphite oxide, which has a substantially higher interlayer spacing of ~0.8 nm.[26]

The majority of the primary nanographitic particles are larger than the microemulsion mean droplet size. This indicates that, as the nanoparticles grow, the surrounding sulfuric acid and surfactant film can distort so as to accommodate this growth with additional sulfuric acid and surfactant being supplied by impinging and fusing microemulsion droplets. Expulsion of the 3−30 nm nanoparticles from the droplets as bare particles into the cyclohexane continuous phase can be ruled out because this would not support stacking with the crystallographic registry; rather, a polycrystalline aggregate of the primary particles would result.

Note that the smallest nanographitic primary particles with size <5 nm are few-layer graphene quantum dots. Owing to their carboxylate decorated edges, these graphene dots show bright green photoluminescence when they are extracted into an aqueous phase from the microemulsions by adding excess water. We are currently using a similar microemulsion methodology to create larger quantities of carbon dots with a narrow size distribution commensurate with the mean microemulsion droplet size (Figure S7). Here, however, the emphasis is on showing that some of these primary particles stack in a crystallographic registry to produce much larger nanographitic aggregates similar to mesocrystals. These larger ~250 nm- to μm-sized particles can form within a day in the microemulsions.

Mesocrystal-like Nanographitic Aggregates. The larger ~250 nm graphitic aggregates imaged by TEM show hexagonal facetting and clear evidence of the smaller ~3−30 nm nanographitic particle stacking on their surfaces and edges (Figure 4a,b and Figure S3); primary particles also typically surround the larger ~250 nm aggregates, corroborating the origin of the latter. In early stages of development, these aggregates can appear holey and fragmented but nevertheless still produce single crystal-type electron diffraction patterns (Figure 4b). With further attachment of primary particles, μm-sized thicker aggregates eventually form (Figure 4c and Figure S4). Importantly, these μm-sized particles produce the typical single crystal diffraction expected for graphite with ordered AB Bernal stacking rather than the random stacking of turbostratic graphite, which would produce diffraction rings. In addition, the diffraction spots are sharp, revealing that the primary nanoparticles stack in a crystallographic registry, i.e., structures resembling mesocrystals have formed. This again demonstrates that the stacking is well-controlled; the primary ~3−30 nm nanographitic particles only stack irreversibly when their lowest energy stacking arrangement has been attained, thereby producing mesocrystalline-like nanographite rather than polycrystalline or turbostratic aggregates.

The graphite particles of size ~0.25−1 μm are typically faceted (Figure 4a,c and Figures S3 and S4), whereas the larger μm-sized particles often have a more irregular shape, reflecting the larger size and shape differential in their nanographitic building blocks, as shown by AFM and ESEM images (Figure 5 and Figure S8).

Comparison of Low and High Sucrose Content Microemulsions. It is important to emphasize that the mesocrystal-like nanographitic aggregates and their smaller ~3−30 nm primary particles are the main product from our microemulsions only when the sucrose concentration is kept at or below 1 wt %. In particular, there is increasing variability in the product quality as the sucrose concentration rises from 1 to 30 wt %. At 30 wt % sucrose concentration, the main product is amorphous humin, but carbon nano-onions showing the 0.34 nm interlayer spacing also form (Figure S9), whereas the graphitic nanocrystals are seen more rarely.

The product variability when higher sucrose concentration microemulsions are used reflects the distribution of reactants

DOI: 10.1021/acs.cgd.5b01753
Cryst. Growth Des. 2016, 16, 3133−3142

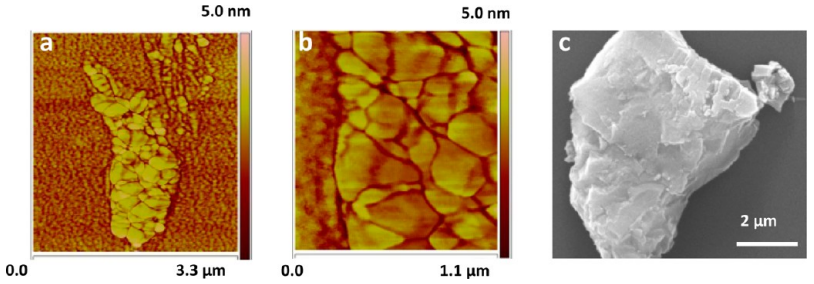

Figure 5. Representative AFM images and ESEM micrograph of the μm-sized nanographitic particles synthesized from 0.25 to 1 wt % aqueous sucrose and sulfuric acid-mixed microemulsions. (a,b) AFM phase contrast images from a 3 μm graphitic particle, revealing its constituent nm-sized particles; (b) shows a region from (a) at higher magnification. (c) ESEM micrograph revealing multiple steps and constituent particles on the surface of a 10 μm graphitic particle.

among the droplets and, to a lesser extent, the deviation in the microemulsion droplet size. Microemulsions are known to be relatively monodisperse,[29] and this will remain true even as the synthesis proceeds because only a tiny proportion of the droplets will contain the larger carbonaceous particles that are likely to distort their dimensions significantly from their preferred curvature size (this distortion being a lower energy cost than expelling the particle from the droplet into the continuous oil phase). Hence, to a first approximation, the microemulsions can be modeled as monodisperse droplets with an initial Poisson distribution of sucrose molecules among the droplets.[30]

The mean radius of the droplets' hydrophilic core is 1.9 nm, giving a nominal mean number of sucrose molecules per droplet of 0.07 for the 1 wt % sucrose microemulsions; thus, most droplets will not contain carbon particles. Pristine graphene sheets of size 1−2 nm would require dehydration and polymerization of ∼4−16 sucrose molecules. For a Poisson distribution of sucrose molecules, 4 sucrose molecules would occur in ∼1 in 10^6 microemulsion droplets, whereas 16 sucrose molecules would only arise in ∼1 in 10^{32}. In our 2 g standard microemulsion size, there are ∼10^{18} droplets. This highlights that 2 nm-sized carbonaceous particles are unlikely to arise in the 1 wt % sucrose microemulsion droplets without additional sucrose acquisition through transient droplet dimer formation. Once formed, these particles will acquire additional reactants through droplet dimer formation at such a slow rate that the particles are bathed in sulfuric acid for sufficient time to become virtually pristine graphene sheets.

In contrast, for 30 wt % sucrose concentrations, the mean number of sucrose molecules per droplet is 2; 4 sucrose molecules would occur in 1 in 10 microemulsion droplets, and 16 sucrose molecules would arise in 1 in 10^{10} droplets. Consequently, there are likely to be ≥10^8 2 nm particles in our standard 2 g mixed microemulsions soon after mixing, and these will then grow relatively rapidly as they acquire more reactants through transient droplet dimer formation. Hence, the droplets containing more sucrose can grow sheets that are large enough to stack irreversibly even when they contain residual oxygen and hydrogen, thereby producing humins.

Comparison of Raman, XRD, and TEM Data. The position, relative intensity, and fwhm of the Raman D, G, and 2D peaks of carbonaceous particles are useful in determining the size, L, of graphene domains and the extent of defects. In particular, for graphene domains of size <3 nm, the D peak intensity increases with crystallite size so that I_D/I_G is considered proportional to L^2, and the D, G, and 2D bands are significantly broadened.[31−33] Raman spectra from isolated particles from the microemulsions that adhered onto silicon wafers suffered from poor signal-to-noise (Figure 6) because of their tiny nm to μm size. In addition, the spectra were dominated by the underlying silicon wafer to the extent that the Si third order peak at 1450 cm^{-1}[34] made a significant contribution to the D and G peak regions. Hence, reliable fwhm and I_D/I_G values could not be obtained, and the 2D peak was barely discernible. Nevertheless, it is clear from the breadth of the D, G, and 2D peaks that the intrasheet graphene domains in the particles have a mean size of ≤2−3 nm.

The quantity of the nanographitic product obtained using the mixed microemulsion approach was limited because the sucrose solutions were restricted to 0.25−1 wt % in the aqueous phase to ensure a mainly nanographitic product. Attempts to extract and isolate the nanographitic product from the microemulsions by using ultracentrifugation and rotary evaporation failed because the solid product was overwhelmingly the surfactant CTAC, which was not surprising given that the mass ratio of surfactant to sucrose was more than 400:1 (Table S1). This meant XRD analysis could not be performed on the nanographitic product synthesized using the mixed microemulsion methodology. An increase in the quantity of carbonaceous product, albeit with decreased crystallinity, could be achieved by modifying the synthesis methodology. In particular, instead of using a sucrose microemulsion, 2 mg of sucrose crystals per gram of microemulsion were added to a sulfuric acid microemulsion and left to slowly dissolve, which took ∼1−2 weeks. A black precipitate emerged after ∼3−4 weeks.

In this experimental setup, the sucrose dehydration reaction can proceed via two routes. First, slow dissolution of the sucrose crystals can occur through the continuous phase into the sulfuric acid droplets, where the dehydration reaction then proceeds. Second, droplets can collide and rupture onto the sucrose crystals, releasing sulfuric acid directly onto the sucrose to produce amorphous carbon and humins, as in the bulk sucrose and sulfuric acid reaction; this mechanism was particularly noticeable for microemulsions containing 60 μL of sulfuric acid per gram of surfactant solution. Note that this sucrose crystal dissolution methodology inherently suffers from the disadvantages of long synthesis time and contamination with amorphous content, and thus, it was used only to produce sufficient material for XRD and Raman analysis to corroborate our findings from the mixed sucrose and sulfuric acid microemulsion methodology.

The XRD of the black product that was obtained in a month by using 50 μL of sulfuric acid per gram of surfactant solution to form the microemulsion and then adding 2 mg g^{-1} of sucrose is shown in Figure 7 and Figure S10f. The graphite (002) peak is not discernible above the broad amorphous peak centered

DOI: 10.1021/acs.cgd.5b01753
Cryst. Growth Des. 2016, 16, 3133−3142

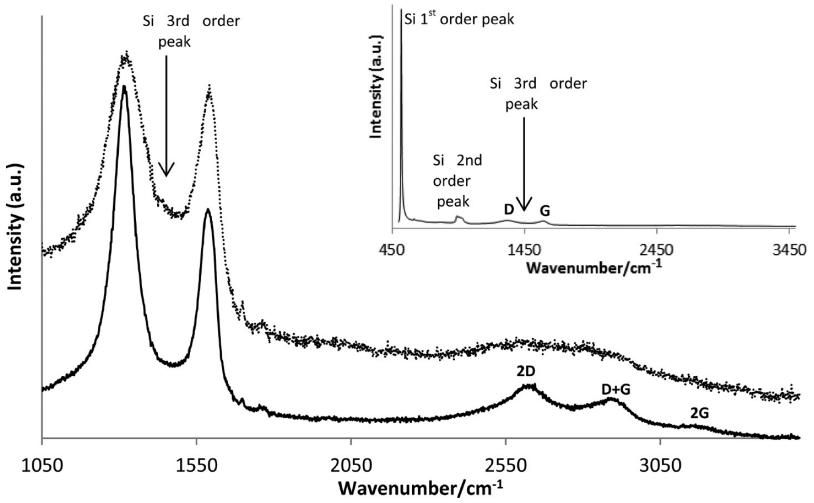

Figure 6. Raman spectra of the nanographitic aggregates. Spectrum from a 3 μm particle synthesized from 1 wt % of aqueous sucrose and sulfuric acid-mixed microemulsion (gray curve). The D peak at ∼1350 cm^{-1} also contains a significant contribution from the supporting silicon wafer's 3rd order peak at ∼1450 cm^{-1}.[34] The inset highlights that the peaks from the 3 μm particle are very weak compared to those of the supporting silicon wafer's 1st order peak. The black curve shows the spectrum of the black precipitate from the microemulsion containing 45 μL g^{-1} sulfuric acid with 2 mg g^{-1} added sucrose crystals and has D, G, 2D, D+G, and 2G peaks.

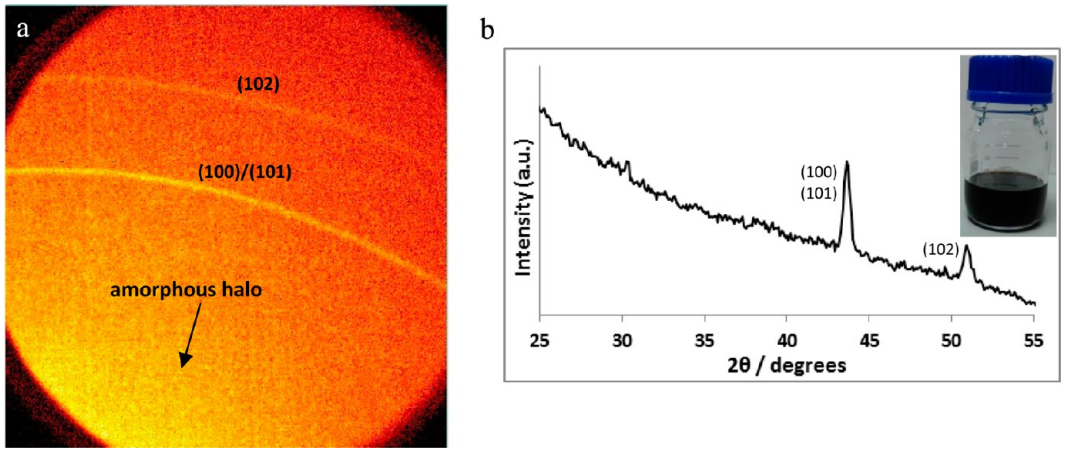

Figure 7. XRD data from the precipitate of the microemulsion containing 50 μL g^{-1} of sulfuric acid and 2 mg g^{-1} of sucrose crystals. (a) Two-dimensional XRD detector image and (b) Chi scan of (a). The inset shows that the microemulsion has turned black in a month due to the quantity of primary particles it contains, whereas the mixed microemulsions containing 1 wt % aqueous sucrose remained colorless in this time frame.

at $2\theta \approx 21°$, but the graphite (100)/(101) peak (2θ = 43.8° corresponding to a mean spacing of 0.207 nm) and a weaker (102) peak (2θ = 51.0° corresponding to a spacing of 0.179 nm) are clearly visible and relatively sharp; the fwhm values are relatively low at 0.4° for the (100)/(101) peak and 0.6° for the (102). Indeed, the peaks are much sharper than would be expected for diffraction from just our primary nanographitic particles; turbostratic packing of 3 nm nanographitic particles would give a (100) peak with a fwhm of ∼5° using the Scherrer equation and a shape factor of 1.84, which is more appropriate for 2D crystallites.[35,36] The (102) peak clearly establishes that graphitic AB stacking has occurred; turbostratic stacking would produce only (hk0) and (002l) peaks. Application of the Scherrer equation with a shape factor of 0.9 to the (102) peak gives an estimated crystallite size of ∼15 nm in this direction, corresponding to ∼8 nm in the intersheet c-direction and equating to ∼23 stacked graphene sheets. This crystallite size is likely to be the minimum value because it is well-known that lattice distortions (likely to be present in our samples due to the presence of some furan rings as well as arenes) also lead to XRD peak broadening.[21] The 15 nm crystallite size shows that the primary nanographite building blocks, which have intersheet sizes of only a few nm, must have stacked with a crystallographic registry. Longer XRD runs also reveal a weak (004) peak (Figure S10f). TEM analysis confirmed the presence of nanographitic particles with the expected hexagonal 0.213 nm spacing and intersheet 0.34 nm spacing together with significant quantities of amorphous carbon (Figure S10a–e). The amorphous carbon material is likely to arise from the droplets rupturing onto sucrose crystals, thereby releasing sulfuric acid directly onto the sucrose.

The Raman spectrum of this 2 mg g^{-1} sucrose, 50 μL g^{-1} sulfuric acid sample (Figure S10g) shows significant overlap of the D and G bands, which occur at 1370 and 1580 cm^{-1}, respectively. There is no discernible 2D peak, only a broad hump between 2000 and 3000 cm^{-1}. This also highlights that the sample contains substantial quantities of sp2 amorphous carbons, which produce a G band at a significantly lower wavenumber of ∼1510 cm^{-1},[31,32] and thus increased intensity between the nanographite D and G bands. The I_D/I_G values

DOI: 10.1021/acs.cgd.5b01753
Cryst. Growth Des. 2016, 16, 3133−3142

of ∼0.8 found for this sample reveal a mean graphene domain size of only ∼1 nm.[37] Indeed, although the XRD showed evidence of ordered stacking of the primary nanographitic particles to give some graphite crystallite sizes of ∼20 nm, the Raman is insensitive to this and is swamped by the signals due to the amorphous carbons in the same region. Hence, the spectrum is similar to that obtained from purely amorphous carbonaceous product synthesized from the bulk reaction.

By reducing the sulfuric acid quantity further to 45 μL g^{-1} in the microemulsion while retaining the sucrose quantity of 2 mg g^{-1}, substantially less precipitate (<10 mg from a 100 mL microemulsion) is produced within 1 month, though the microemulsion still turns black, showing that many nanographitic primary particles remain dispersed throughout the microemulsion. The microemulsion droplets have a mean hydrophilic core radius of ∼1.9 nm, similar to that of the 50 μL g^{-1} sulfuric acid microemulsion, but they contain less of the cosurfactant pentanol (Supporting Information SAXS results and Figure S1); consequently, the interfacial film is less flexible.[38,39] This decreased flexibility reduces the rate at which sucrose molecules diffuse from the continuous phase into the droplet interior and the rate of droplet dimer formation; both of these factors slow the nanographite formation rate. Crucially, though, the rate at which droplets rupture onto sucrose crystals is also significantly reduced, and this factor ensures a higher proportion of nanographite to amorphous content in the precipitate. The increased proportion of nanographitic material results in the (002) peak at 2θ = 25.9° now being clearly seen above the much weaker amorphous halo at 2θ = 21.2°, though the lack of precipitate means only an isolated diffraction spot rather than a continuous ring is observed due to their being insufficient crystallites for all orientations to be present (Figure 8 and Figure S11). The 2θ value of 25.9° corresponds to a mean interplanar spacing of 0.344 nm, which is only slightly larger than the 0.335 nm value for graphite. For longer exposure times, a (100) signal emerges above the signal noise (Figure S11b). Application of the Scherrer equation to the (002) and (100) peaks gives minimum intersheet and intrasheet crystallite sizes of ∼30 and ∼25 nm, respectively, again suggesting mesocrystalline-like nanographite formation. TEM analysis of drops of the microemulsion deposited onto TEM grids shows that the majority of the carbonaceous product that has not precipitated consists of the small ∼3−30 nm primary nanographitic particles shown in Figure 3.

For the 2 mg g^{-1} of sucrose, 45 μL g^{-1} of sulfuric acid sample, the Raman D and G peaks were at 1316 and 1585 cm^{-1}, respectively, and the 2D peak was also clearly visible at 2630 cm^{-1} along with the D + G peak (2900 cm^{-1}) and a weak 2G (3170 cm^{-1}) peak (Figure 6). The fwhm of the G peak is ∼70 cm^{-1}. This is much larger than the typical values found for μm-sized graphite particles[40,41] but comparable to those of graphite nanoparticles[41,42] and nm-sized graphene'[37,42−44] and suggests that the majority of the sample has graphene domain sizes below 3 nm. The I_D/I_G value of 1.8 substantiates this, giving a mean graphene domain size of ∼2 nm.[37] Note that the Raman data reveals the characteristics of the primary building blocks because the in-plane crystallite size measured by Raman data is the mean distance between defects, i.e., it is the mean graphene domain size L, whereas the electron and X-ray diffraction can reveal the structure of the much larger nanaographite aggregates produced from the crystallographic stacking of the primary building blocks. Consequently, the combined Raman and XRD data shows that the majority of the product from the 2 mg g^{-1} of sucrose, 45 μL g^{-1} of sulfuric acid microemulsion comprises carbons with nanographitic domains of ∼2 nm, some of which stack in a crystallographic registry to produce graphite crystallite sizes of ∼20−30 nm. All of the experimental evidence therefore suggests that the larger particles are formed mainly from the stacking of primary nanographitic particles rather than their fusion into larger continuous sheets. Hence, the mean graphene domain size (∼2 nm) remains commensurate with the mean size of the microemulsion droplets' hydrophilic core (∼4 nm). An estimate of the likely elemental composition of our nanographitic product, based on the crystallographic stacking of smaller primary particles so that the mean graphene domain size is in the range 1−3 nm, is provided in Tables S4−S6. The estimates suggest the particles contain between 10 and 25% by mass of oxygen, assuming that 1 in every 3 or 1 in every 4 edge carbons is carboxylated.

The TEM, XRD, and Raman data support a microemulsion-mediated synthesis route that produces nanographite at sufficiently low sucrose quantities with increasing amounts of amorphous carbons and humins arising at higher sucrose levels. The nanographite synthesis mechanism involves hierarchal ordering as depicted in Figure 1. Essentially, pristine nanographene sheets are synthesized and undergo ordered stacking

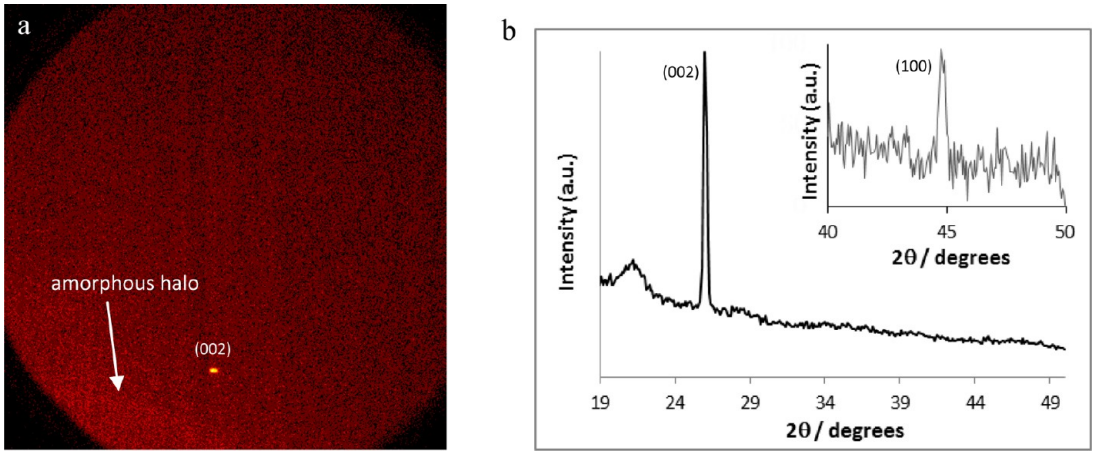

Figure 8. XRD data from <10 mg of nanographitic aggregates precipitated for 1 month from a 45 μL g^{-1} of sulfuric acid microemulsion with 2 mg g^{-1} of added sucrose crystals. (a) Two-dimensional XRD detector image obtained after 2 h showing the (002) peak and a very weak amorphous halo. (b) Chi integration of the data shown in (a). The inset shows the weaker (100), which is observable above the background for longer runs.

DOI: 10.1021/acs.cgd.5b01753
Cryst. Growth Des. 2016, 16, 3133−3142

in the microemulsion droplets to produce primary nanographitic particles of ∼3−30 nm. Some of the primary nanographitic particles then stack to form ∼250 nm nanographitic particles with further stacking ultimately producing μm-sized graphitic particles. These stages will occur concurrently to varying degrees given the distribution of reactants and polydispersity of the microemulsion droplets. The μm-sized graphitic particles therefore resemble mesocrystals; single crystal-like structures produced through the oriented attachment of crystalline nanoparticles. This nonclassical crystallization route differs significantly from previous graphite formation mechanisms of molecule-by-molecule growth during chemical vapor deposition or a solid-state pressure- and temperature-induced graphitization.

CONCLUSIONS

Our microemulsion methodology provides a simple room temperature route for the synthesis of nanographitic particles. The sucrose concentrations in the microemulsion droplets must be kept very low for a mainly nanographitic product to arise; however, this severely limits the nanographite yield. The nanographitic, rather than purely amorphous, product highlights the order that can be imposed on reactions by using microemulsions. The nanographite formation proceeds via a nonclassical crystallization route similar to those of mesocrystals; stacking of nanographene sheets occurs to produce primary nanographitic particles, which then stack in a crystallographic registry to form larger μm-sized particles. Although yields are small, our findings do challenge established thinking that high temperature is a prerequisite for graphite formation.

ASSOCIATED CONTENT

Supporting Information

The Supporting Information is available free of charge on the ACS Publications website at DOI: 10.1021/acs.cgd.5b01753.

Microemulsion compositions, SAXS data and analysis, and additional TEM, Raman microscopy, XRD, fluorescence and AFM data (PDF)

AUTHOR INFORMATION

Corresponding Author

*Tel: +44 (0)191 334 2098. Fax: +44 (0)191 334 2051. E-mail: sharon.cooper@durham.ac.uk.

Notes

The authors declare no competing financial interest.

ACKNOWLEDGMENTS

This work was supported by GSK and the UK Engineering and Physical Sciences Research Council. We thank Prof. Beeby and Dr. Nicholson for Raman microscopy assistance, Drs. Mendis and Thompson for TEM and AFM assistance, respectively, Ms Berry for SAXS measurements, and Profs. Bain, Coleman, and Evans for reviewing this article.

REFERENCES

(1) Wehling, T. O.; Novoselov, K. S.; Morozov, S. V.; Vdovin, E. E.; Katsnelson, M. I.; Geim, A. K.; Lichtenstein, A. I. *Nano Lett.* **2008**, *8*, 173−177.
(2) Lv, R.; Terrones, M. *Mater. Lett.* **2012**, *78*, 209−218.
(3) Edwards, R. S.; Coleman, K. S. *Nanoscale* **2013**, *5*, 38−51.
(4) Li, X.; Rui, M.; Song, J.; Shen, Z.; Zeng, H. *Adv. Funct. Mater.* **2015**, *25*, 4929−4947.
(5) Kwiecinska, B.; Petersen, H. I. *Int. J. Coal Geol.* **2004**, *57*, 99−116.
(6) Fitzer, E.; Köchling, K. H.; Boehm, H. P.; Marsh, H. *Pure Appl. Chem.* **1995**, *67*, 473−506.
(7) Takai, K.; Oga, M.; Sato, H.; Enoki, T.; Ohki, Y.; Taomoto, A.; Suenaga, K.; Iijima, S. *Phys. Rev. B: Condens. Matter Mater. Phys.* **2003**, *67*, 214202.
(8) Patil, S. K. R.; Lund, C. R. F. *Energy Fuels* **2011**, *25*, 4745−4755.
(9) Hoang, T. M. C.; van Eck, E. R. H.; Bula, W. P.; Gardeniers, J. G. E.; Lefferts, L.; Seshan, K. *Green Chem.* **2015**, *17*, 959.
(10) Chuntanapum, A.; Matsumura, Y. *Ind. Eng. Chem. Res.* **2009**, *48*, 9837−9846.
(11) Antal, M. J.; Mok, W. S. L.; Richards, G. N. *Carbohydr. Res.* **1990**, *199*, 91−109.
(12) Franklin, R. E. *Proc. R. Soc. London, Ser. A* **1951**, *209*, 196−218.
(13) Sun, Z.; Yan, Z.; Yao, J.; Beitler, E.; Zhu, Y.; Tour, J. M. *Nature* **2010**, *468*, 549−552.
(14) Li, X.-H.; Kurasch, S.; Kaiser, U.; Antonietti, M. *Angew. Chem., Int. Ed.* **2012**, *51*, 9689−9692.
(15) Sevilla, M.; Sanchís, C.; Valdés-Solís, T.; Morallón, E.; Fuertes, A. B. *Carbon* **2008**, *46*, 931−939.
(16) Anderson, J. M.; Johnson, R. L.; Schmidt-Rohr, K.; Shanks, B. H. *Carbon* **2014**, *74*, 333−345.
(17) Hoekstra, J.; Beale, A. M.; Soulimani, F.; Versluijs-Helder, M.; Geus, J. W.; Jenneskens, L. W. *J. Phys. Chem. C* **2015**, *119*, 10653−10661.
(18) Peng, H.; Travas-Sejdic, J. *Chem. Mater.* **2009**, *21*, 5563−5565.
(19) Liu, H.; Miao, C.; Tang, Z.; Zheng, X.; Qin, X.; Zhang, X. *Mater. Lett.* **2012**, *83*, 62−64.
(20) Dey, R. S.; Hajra, S.; Sahu, R. K.; Raj, C. R.; Panigrahi, M. K. *Chem. Commun.* **2012**, *48*, 1787−1789.
(21) Kim, Y.-Y.; Schenk, A. S.; Ihli, J.; Kulak, A. N.; Hetherington, N. B. J.; Tang, C. C.; Schmahl, W. W.; Griesshaber, E.; Hyett, G.; Meldrum, F. C. *Nat. Commun.* **2014**, *5*, 4341.
(22) Chen, C.; Nicholson, C. E.; Ramsey, H. E.; Cooper, S. J. *Cryst. Growth Des.* **2015**, *15*, 1060−1066.
(23) Brunner-Popela, J.; Glatter, O. *J. Appl. Crystallogr.* **1997**, *30*, 431−442.
(24) Nicholson, C. E.; Chen, C.; Mendis, B.; Cooper, S. J. *Cryst. Growth Des.* **2011**, *11*, 363−366.
(25) Cooper, S. J.; Cook, O. J.; Loines, N. Crystallization in Microemulsions: A Generic Route to Thermodynamic Control and the Estimation of Critical Nucleus Size. In *Crystallization - Science and Technology* [online]; Andreeta, M., Ed.; InTech, 2012: Ch. 5, pp 121−148. http://www.intechopen.com/books/crystallization-science-and-technology/crystallization-in-microemulsions-a-generic-route-to-thermodynamic-control-and-the-estimation-of.
(26) Shao, G.; Lu, Y.; Wu, F.; Yang, C.; Zeng, F.; Wu, Q. *J. Mater. Sci.* **2012**, *47*, 4400−4409.
(27) Behabtu, N.; Lomeda, J. R.; Green, M. J.; Higginbotham, A. L.; Sinitskii, A.; Kosynkin, D. V.; Tsentalovich, D.; Parra-Vasquez, A. N. G.; Schmidt, J.; Kesselman, E.; Cohen, Y.; Talmon, Y.; Tour, J. M.; Pasquali, M. *Nat. Nanotechnol.* **2010**, *5*, 406−411.
(28) Dresselhaus, M. S.; Dresselhaus, G. *Adv. Phys.* **2002**, *51*, 1−186.
(29) Eriksson, J. C.; Ljunggren, S. *Langmuir* **1995**, *11*, 1145−1153.
(30) de Dios, M.; Barroso, F.; Tojo, C.; López-Quintela, M. A. *J. Colloid Interface Sci.* **2009**, *333*, 741−748.
(31) Ferrari, A. C. *Solid State Commun.* **2007**, *143*, 47−57.
(32) Ferrari, A. C.; Robertson, J. *Phys. Rev. B: Condens. Matter Mater. Phys.* **2000**, *61*, 14095−14106.
(33) Cançado, L. G.; Jorio, A.; Pimenta, M. A. *Phys. Rev. B: Condens. Matter Mater. Phys.* **2007**, *76*, 064304.
(34) Casiraghi, C.; Ferrari, A. C.; Robertson, J.; Ohr, R.; Gradowski, M.; Schneider, D.; Hilgers, H. *Diamond Relat. Mater.* **2004**, *13*, 1480−1485.
(35) Warren, B. E.; Bodenstein, P. *Acta Crystallogr.* **1965**, *18*, 282−286.
(36) Warren, B. E. *Phys. Rev.* **1941**, *59*, 693−698.

DOI: 10.1021/acs.cgd.5b01753
Cryst. Growth Des. 2016, 16, 3133−3142

(37) Cançado, L. G.; Jorio, A.; Martins Ferreira, E. H.; Stavale, F.; Achete, A.; Capaz, R. B.; Moutinho, M. V. O.; Lombardo, A.; Kulmala, T. S.; Ferrari, A. C. *Nano Lett.* **2011**, *11*, 3190−3196.
(38) Eastoe, J.; Hollamby, M. J.; Hudson, L. *Adv. Colloid Interface Sci.* **2006**, *128*−*130*, 5−15.
(39) López-Quintela, M. A.; Tojo, C.; Blanco, M. C.; Garćia Rio, L. G.; Leis, J. R. *Curr. Opin. Colloid Interface Sci.* **2004**, *9*, 264−278.
(40) Kwak, J.; Chu, J. H.; Choi, J.-K.; Park, S.-D.; Go, H.; Kim, S. Y.; Park, K.; Kim, S.-D.; Kim, Y.-W.; Yoon, E.; Kodambaka, S.; Kwon, S.-Y. *Nat. Commun.* **2012**, *3*, 645.
(41) Wilhelm, H.; Lelaurain, M.; McRae, E.; Humbert, B. *J. Appl. Phys.* **1998**, *84*, 6552−6558.
(42) Martins Ferreira, E. H.; Moutinho, M. V. O.; Stavale, F.; Lucchese, M. M.; Capaz, R. B.; Achete, C. A.; Jorio, A. *Phys. Rev. B: Condens. Matter Mater. Phys.* **2010**, *82*, 125429.
(43) Sergiienko, R.; Shibata, E.; Kim, S.; Kinota, T.; Nakamura, T. *Carbon* **2009**, *47*, 1056−1065.
(44) Herron, C. R.; Coleman, K. S.; Edwards, R. S.; Mendis, G. M. *J. Mater. Chem.* **2011**, *21*, 3378−3383.

DOI: 10.1021/acs.cgd.5b01753
Cryst. Growth Des. 2016, 16, 3133−3142